JOURNAL OF APPLIED ELECTROCHEMISTRY 24 (1994) 131–138

# Local structure and concentration in Al–Mn alloy electrodeposits

T. TAKAYAMA, H. SETO, J. UCHIDA, S. HINOTANI

*Iron and Steel Research Laboratories, Sumitomo Metal Industries Ltd, 1-8, Fusocho, Amagasaki, Hyogo, 660 Japan*

Received 6 February 1992; revised 28 May 1993

The structures of f.c.c. crystalline and amorphous phases coexisting in Al–Mn alloy electrodeposits containing 11–30 wt % were examined by using the grazing-incidence X-ray diffraction (GIXD) method, high-resolution transmission electron microscopy combined with energy dispersive X-ray spectrometry (HRTEM/EDS), and the manganese *K*-edge extended X-ray absorption fine-structure (EXAFS) technique. The amorphous and f.c.c. phases were homogeneously distributed in the through-thickness direction of the electrodeposits, although the amorphous phase increased and the f.c.c. phase decreased with increasing manganese total concentration. The decrease of Mn-content in the f.c.c. crystalline phases with increasing manganese total concentration was revealed by the lattice constant measurement of the f.c.c. crystalline phase. This result was also supported by the microarea elemental analysis by HRTEM/EDS. The EXAFS result has indicated that the manganese local structures in the amorphous phases are almost identical in different manganese total concentration electrodeposits. This suggests that the Mn-content in the amorphous phases hardly changes with increasing manganese total concentration. These results have revealed that a peculiar elemental partition occurs in the amorphous and crystalline phases of Al–Mn alloy electrodeposits.

## 1. Introduction

Al–Mn alloys have been produced by melt quenching [1, 2], sputtering [3], electrodepositing [4–7], and other techniques. Among the production methods, electrodeposition is especially interesting as an industrial process for highly corrosion-resistant coatings. In electrodeposition from aluminium chloride electrolytes at 423 K, the structure of Al–Mn alloys containing up to 50 wt % Mn have shown that the lower manganese alloys consist of the f.c.c. crystalline phase, and the compositional limit of manganese in the f.c.c. phase is extended to 9 wt % Mn more than that in the equilibrium Al–Mn phase diagram [8]. With additional manganese, the amorphous phase appears and the f.c.c. phase decreases [5, 6]. Completely amorphous electrodeposition is obtained in the composition range between 26 and 39 wt % Mn [9]. At higher manganese concentration, the amorphous phase is gradually replaced by a b.c.c. crystalline phase [5].

As mentioned above, the structure of electrodeposited Al–Mn alloys is different from Al–Mn equilibrium phases [8] and also from those obtained by melt quenching [1, 2]. In melt quenching foils, the amorphous phase appears at a concentration of 26.4 wt % Mn. The lower and higher manganese alloys consist of icosahedral and decagonal type quasicrystalline phases, respectively. The local structure of the amorphous phase has been revealed by the extended X-ray absorption fine-structure (EXAFS) method [1, 2].

Grushko and Stafford have also investigated the structures of Al–Mn alloys electrodeposited at elevated temperatures and quasicrystalline phases, such as icosahedral and decagonal, have been shown to appear at 598 K [7].

In this work, Al–Mn alloys (11–30 wt % Mn total concentration) electrodeposited at a molten salt temperature of 473 K were examined with emphasis on the local structure and concentration by using the grazing-incidence X-ray diffraction (GIXD) method, high-resolution transmission electron microscopy (HRTEM) combined energy dispersive X-ray spectrometry (EDS), and the manganese *K*-edge EXAFS technique with synchrotron radiation.

## 2. Experimental details

### 2.1. *Materials*

Al–Mn films were electrodeposited on cold-rolled steel sheets from eutectic molten salts of $AlCl_3$(~ 76 wt %)–NaCl–KCl–$MnCl_2$. The Mn-content in the film was controlled by the amount of $MnCl_2$ in the salt mixture [9, 10]. The melting point of the salt mixture was approximately 373 K. The surfaces of the steel substrates were pretreated by anodic activation in the molten salts, in order to obtain good contact between the films and the steel surfaces. Electrodeposition was

0021-891X 

carried out at a salt temperature of 473 K, a salt flow rate of 0.7 m $s^{-1}$, and an electrodeposition current density of 40 A $dm^{-2}$. A final film thickness of about 6 $\mu$m was obtained. The manganese total concentrations in the four deposits were determined to be 11.2, 16.4, 26.3 and 30.0 wt % by inductively coupled plasma atomic emission spectrometry, after complete dissolution in hydrochloric acid. For the reference sample of GIXD and EXAFS measurement, orthorhombic phase $Al_6Mn$ was prepared by thermal annealing, the film containing 26.3 wt % Mn at 673 K for 600 s.

### 2.2. *Apparatus*

The GIXD of Al–Mn films was measured with a Geigerflex Rad-B spectrometer (Rigaku Corporation) combined with the thin-film measuring system with a flat (0002)-graphite monochromator (Model 2655A1) [11]. The rotating cobalt anode was operated at 30 kV and 100 mA. GIXD measurement conditions were an incident slit width of 0.2 mm, a fixed glancing angle ($\alpha$) between 0.2 and 2.0 degrees, and a diffraction angle ($2\theta$) scanning speed of 2 degree $min^{-1}$.

The electron microbeam diffraction (EMD) and/or the microarea elemental analysis (MEA) of Al–Mn films were taken by a 200 kV HRTEM, JEM-2010UHR (JEOL), with a Si(Li)-solid state detector. The electron beam spot size for EMD and MEA was about 10 nm in diameter. For EMD and MEA, the Al–Mn electrodeposits were thinned by a twin-jet electrolysis method with an electrolytic solution of 10 vol % perchloric acid, 20 vol % glycerol, and 70 vol % ethanol. The quantitative MEA was carried out by the standardless correction method in Link QX2000J–T programs, after counting an X-ray spectrum.

The manganese *K*-edge EXAFS spectra were obtained by using a synchrotron radiation beam line operated by Toray Research Center Inc. in the Photon Factory at the National Laboratory of High Energy Physics (KEK, Tsukuba, Japan). The EXAFS spectra of Al–Mn films and reference sample $Al_6Mn$ were measured with the transmission mode, by employing the beam line 7C with a silicon (1 1 1) double crystal monochromator (detuning rate of 70% to remove higher order diffraction beams) combined with a rotary encoder under the storage ring operating condition of 2.5 GeV. The energy resolutions were 0.5 eV for the X-ray absorption near-edge structure (XANES) scanning and 4 to 7 eV for the EXAFS scanning. The EXAFS spectra were analysed by procedures based on single-electron single-scattering theory [12–14]. In the curve fitting, to obtain the structure factors as a distance from the manganese atom to neighbouring atoms ($R$) and the number of neighbouring atoms ($N$) from the EXAFS spectra, correction factors were determined by using the reference material $Al_6Mn$.

## 3. Results

### 3.1. *GIXD profiles of Al–Mn films*

In the 10–25 wt % Mn concentration region of the Al–Mn electrodeposition, dual phase deposition of the f.c.c. lattice phase like Al-crystal and the amorphous phase is known by general X-ray diffraction techniques ($2\theta$–$\theta$ method) [6, 9, 10]. Al–Mn electrodeposits in the dual phase region were measured by GIXD, being more sensitive to the near-surface. The GIXD profiles at $\alpha = 1.0°$ are shown in Fig. 1. The profile of the orthorhombic phase $Al_6Mn$ is shown as the reference in Fig. 1(e). The profiles in Fig. 1 demonstrate the X-ray intensities scattered from the films alone without the steel substrates. In Fig. 1(a)–(d), the intensity of the f.c.c. crystalline phase diffraction peaks indicated by Miller indices decreases, while the intensity of the amorphous halos increases with increasing manganese total concentration. The sample containing 30 wt % Mn is fully amorphous.

Lattice constants of the f.c.c. crystalline phases in Al–Mn films were determined by calculation using GIXD peak positions. The average lattice constants of the f.c.c. crystalline phases are listed in Table 1. The lattice constant of the f.c.c. phase in the 11.2 wt % Mn total concentration sample is smaller than that in the higher manganese total concentration samples.

As a function of glancing angle, the multiple plots of GIXD profiles obtained from two samples of 11.2 and 26.3 wt % Mn total concentration are shown in Fig. 2. The integrated intensities of f.c.c. (1 1 1)-peak

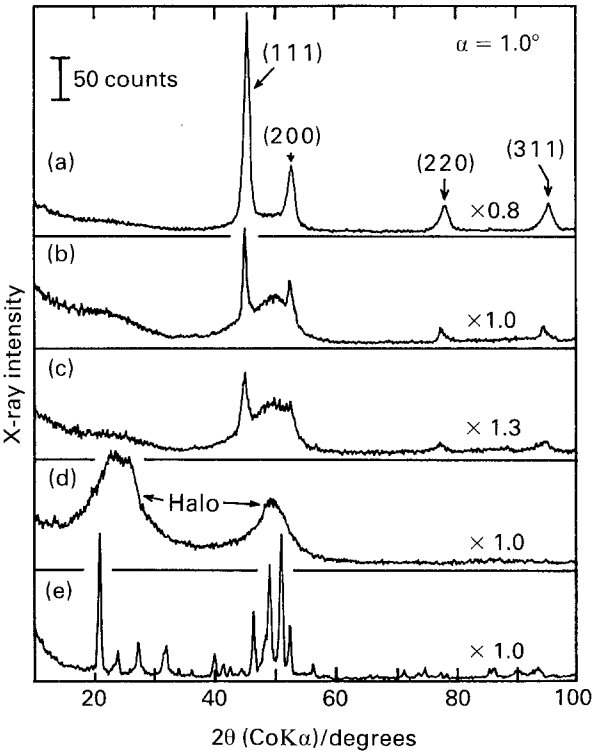


Fig. 1. GIXD profiles of Al–Mn alloy electrodeposits at glancing angle ($\alpha$) of 1.0°. (a) Mn 11.2 wt %; (b) Mn 16.4 wt %; (c) Mn 26.3 wt %; (d) Mn 30.0 wt %; and (e) $Al_6Mn$.

*Table 1. Average lattice constant of f.c.c. crystalline phases in Al–Mn alloy electrodeposits*

| Mn total-concentration (wt %) | 11.2 | 16.4 | 26.3 |
|---|---|---|---|
| f.c.c. lattice constant (nm) | 0.4021 | 0.4046 | 0.4045 |

and amorphous halo near $2\theta = 50°$ and the calculated X-ray penetration depths [15] are displayed in Fig. 3. Distributions of the f.c.c. and amorphous phases in Al–Mn electrodeposition films are discussed in the next section.

### 3.2. *Microarea images and microanalysis of Al–Mn films*

The microdistribution of the f.c.c. crystalline and amorphous phases was observed by HRTEM. The microarea images are shown in Figs 4 to 6. The white regions, such as the D-parts in Figs 5 and 6, are probably the f.c.c. crystalline phases dissolved by the selective electrolysis, in the preparation of thin films.

Two kinds of crystalline phases coexist in the electrodeposition films containing 11.2 and 16.4 wt % Mn, as a result of EMD patterns. One is the conglomerate f.c.c. crystalline, which is polycrystalline with several orientations, such as the A-parts in Figs 4 and 5. The other is the small island-crystalline surrounded by amorphous phases such as the B-parts in Figs 4 and 5. In Fig. 6, the weak spots, which correspond to the (1 1 1)-reflections from the f.c.c. crystalline phases, also appear inside the halo ring in the selected-area diffraction (SAD) pattern, although the distinct indices of the crystalline phase are not shown.

The two kinds of crystalline phases and the amorphous phase were elementally analysed by MEA.

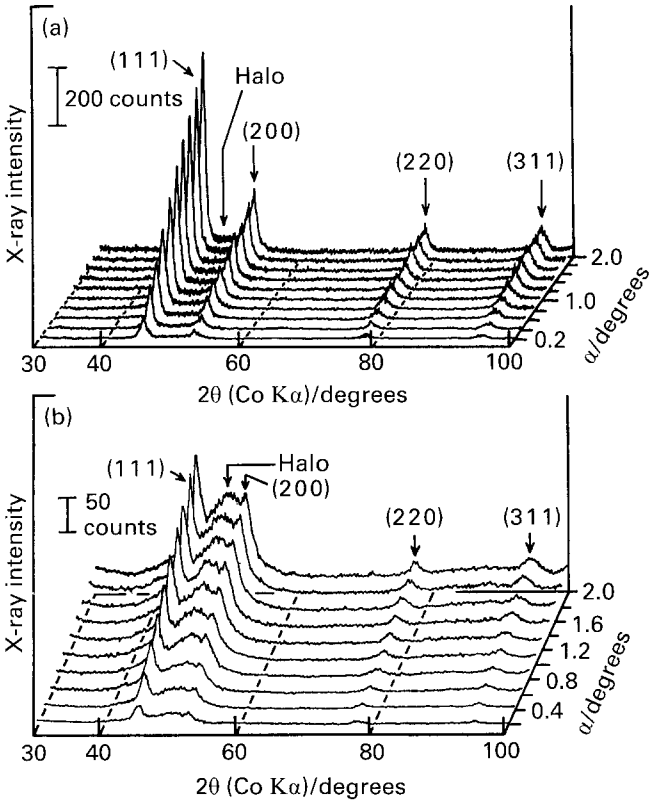


Fig. 2. GIXD profiles of 11.2 and 26.3 wt % Mn total concentration samples as a function of glancing angle ($\alpha$). (a) Al–11.2 wt % Mn; and (b) Al–26.3 wt % Mn.

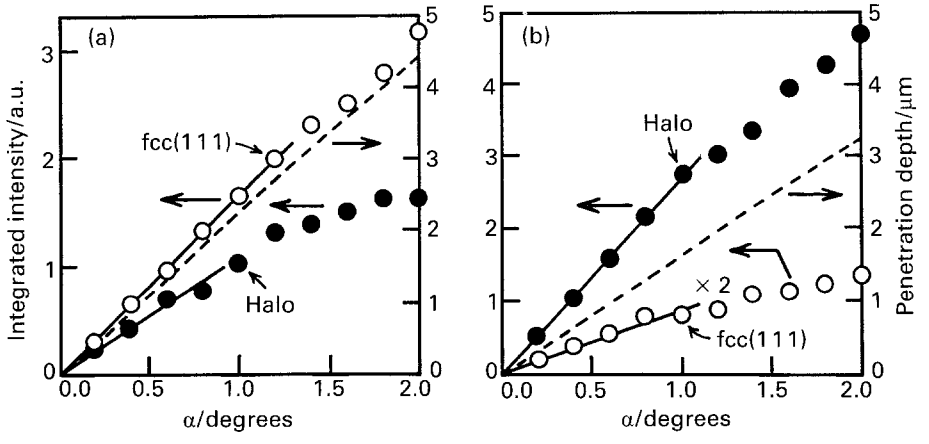


Fig. 3. Integrated intensities of f.c.c. (1 1 1)-peak and amorphous halo near $2\theta = 50°$ and the calculated penetration depths as a function of glancing angle ($\alpha$). (a) 11.2 wt % and (b) 26.3 wt % Mn total concentration samples.

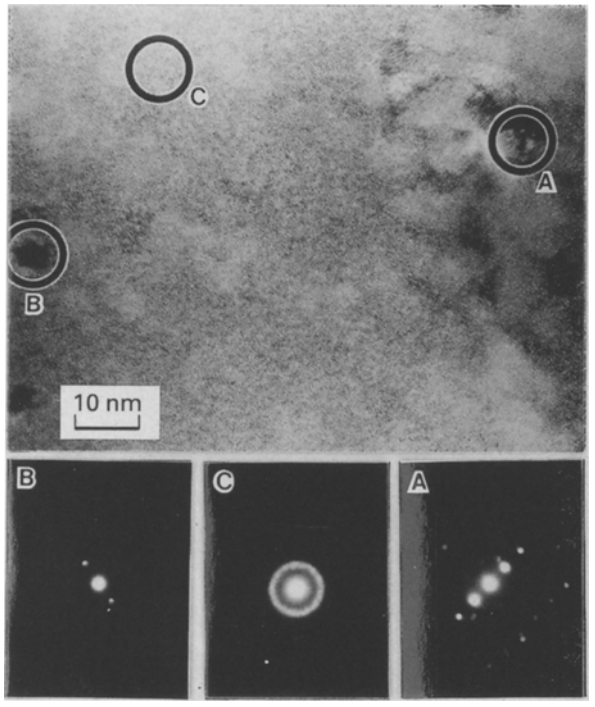


Fig. 4. TEM images and electron diffraction patterns of 11.2 wt % Mn total concentration sample.

The result plotted as a function of manganese total concentration is shown in Fig. 7. The manganese microarea concentration in the conglomerate f.c.c. crystalline phase decreases with increasing manganese total concentration in Fig. 7. The manganese microarea concentration in the small island-crystalline phase surrounded by the amorphous phase increased with increasing manganese total concentration, such as that in the amorphous phase. However, the microarea concentration variation of

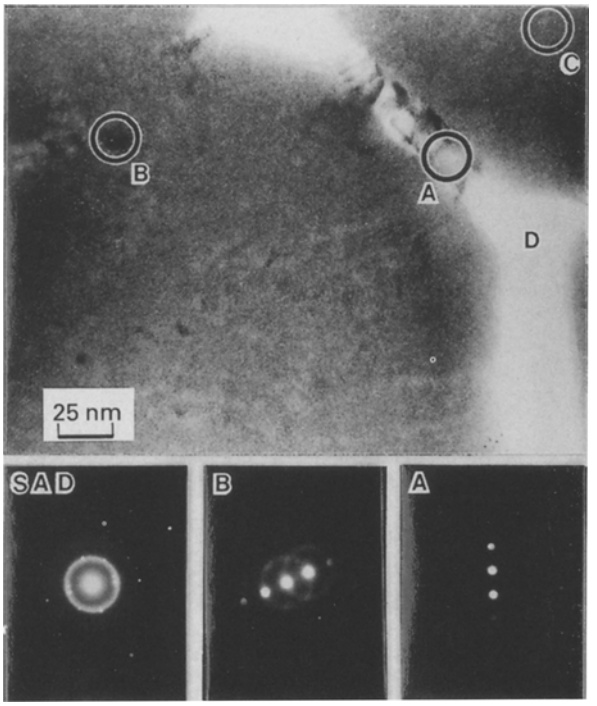


Fig. 5. TEM images and electron diffraction patterns of 16.4 wt % Mn total concentration sample.

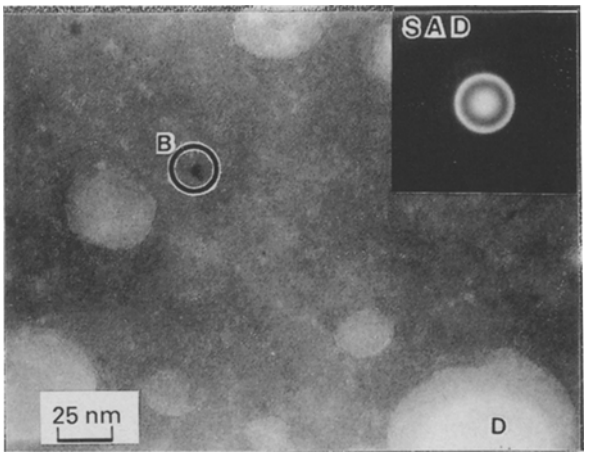


Fig. 6. TEM images and electron diffraction pattern of 26.3 wt % Mn total concentration sample.

the small island crystalline is not shown in Fig. 7, because they embed in the amorphous phase and the values of manganese concentration are ambiguous due to the overlap of the crystalline and amorphous phases.

The manganese microarea concentration in the amorphous phase increases with increasing Mn total concentration. The manganese microarea concentration varies only several weight percent in the manganese total concentration region of 11.2–26.3 wt %.

### 3.3. *X-ray absorption spectra of Al–Mn films*

The net manganese *K*-edge XANES spectra of Al–Mn alloy electrodeposits are shown in Fig. 8. In Fig. 8, the XANES spectrum of the 26.3 wt % Mn total concentration sample corresponds to the 30.0 wt % Mn sample, and the spectrum of $Al_6Mn$ resembles the spectra of 26.3 and 30.0 wt % Mn samples. The XANES spectrum has been recently explained as arising from effects such as photoelectron multiple scattering, many-body interactions, distortion of the

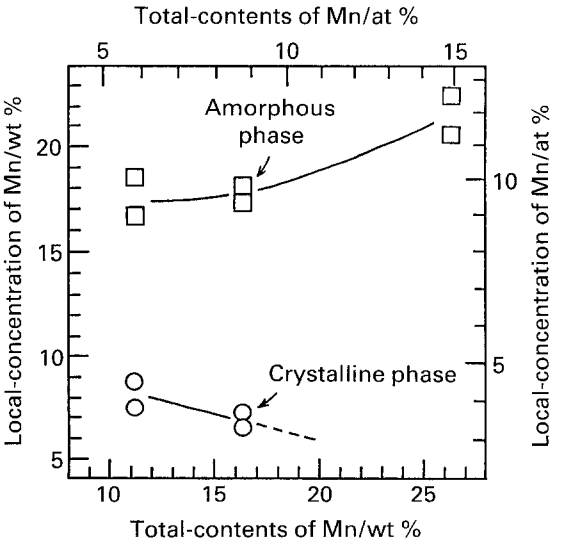


Fig. 7. Local concentration of manganese in f.c.c. and amorphous phases as a function of manganese total concentration.

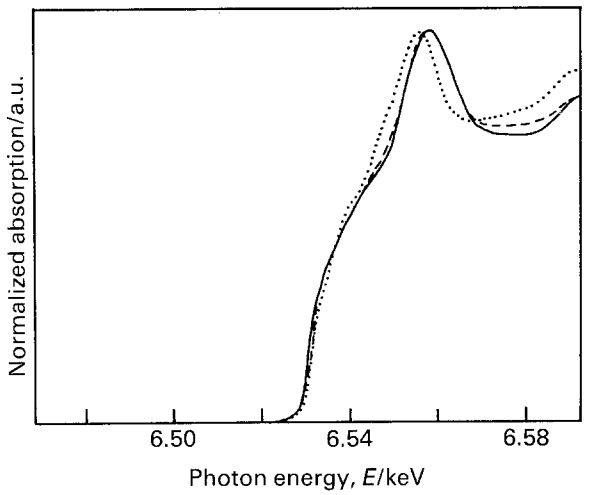


Fig. 8. Manganese *K*-edge XANES spectra of Al–Mn alloy electrodeposits. (····) Al–11.2 wt % Mn; (- - - -) Al–26.3 wt % Mn; (— — —) Al–30.0 wt % Mn; and (——) $Al_6Mn$.

excited state wave function by the Coulomb field band structures, etc. [16] However, XANES spectra have been qualitatively employed as, for example, an indication of three-dimensional structure in complex chemistry [17], such as the fingerprint region in infrared absorption spectrometry. This fingerprint comparison implies that the surrounding structure of manganese atoms in the 26.3 wt % Mn sample almost corresponds to that in the 30.0 wt % Mn sample and resemble orthorhombic $Al_6Mn$, having

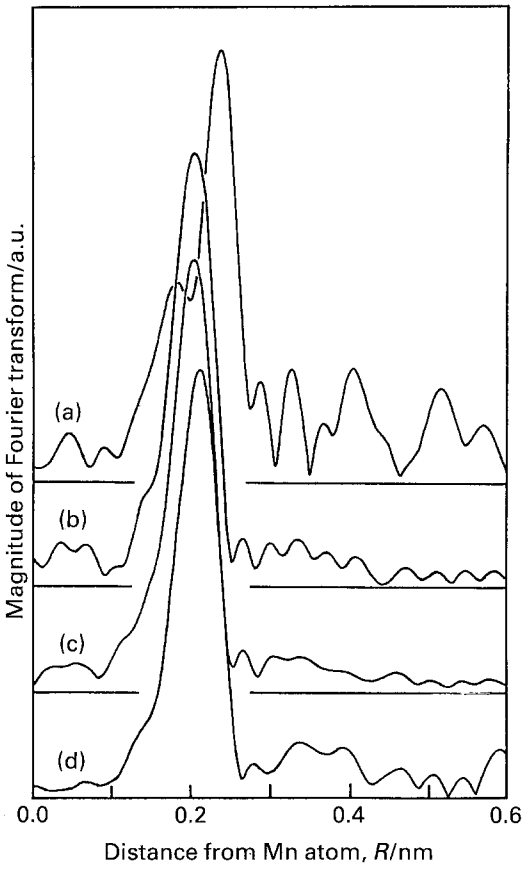


Fig. 10. Radial distribution function of Al–Mn alloy electrodeposits. (a) Al–11.2 wt % Mn; (b) Al–26.3 wt % Mn; (c) Al–30.0 wt % Mn; and (d) $Al_6Mn$.

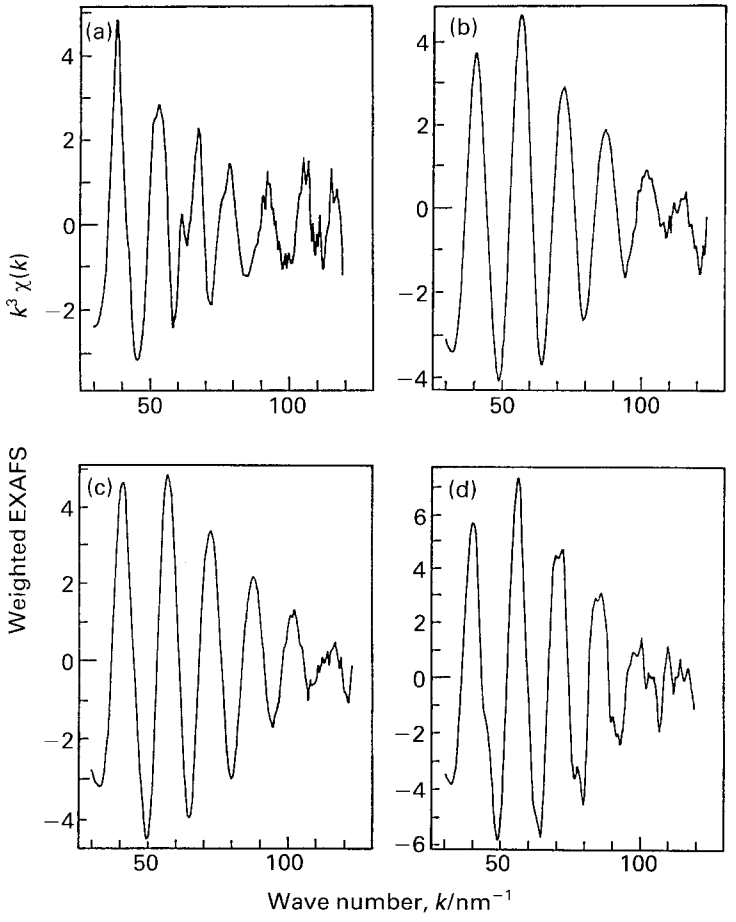


Fig. 9. Extracted manganese *K*-edge EXAFS spectra of Al–Mn alloy electrodeposits. (a) Al–11.2 wt % Mn; (b) Al–26.3 wt % Mn; (c) Al–30.0 wt % Mn; and (d) $Al_6Mn$.

ten nearest aluminium atoms at an average distance of 0.256 nm [18].

The extracted EXAFS spectra and the radial distribution functions (RDF) of Al–Mn electrodeposits and $Al_6Mn$ obtained by the procedures in the previous chapter are shown in Figs 9 and 10, respectively. In Figs 9 and 10, the extracted EXAFS spectrum and the RDF of the 26.3 wt % Mn total concentration sample containing the f.c.c. phase indicate identical profiles with those of the 30.0 wt % Mn sample of the fully amorphous phase. Though the EXAFS spectrum of the 16.4 wt % Mn sample is not shown in Fig. 9, the spectrum corresponded to that of the 26.3 wt % Mn sample. Their EXAFS spectra and RDFs confirm that the aluminium or manganese atom distribution neighbouring on a manganese atom in the 16.4 wt % Mn sample is almost identical to that in the 26.3 wt % Mn sample. Thus, the amorphous phases in both samples contain almost an identical manganese local concentration, although the samples contain different manganese total concentrations. On the other hand, the RDF of the 11.2 wt % Mn total concentration sample shows a similar profile to that of the f.c.c. crystalline phase in Fig. 10(a), because the sample involves large volume of f.c.c. crystalline phase containing manganese. However, the side-peak based on the amorphous phase appears as the shoulder of the major peak at an $R$ of about 0.18 nm.

The structure factors of 26.3 and 30.0 wt % Mn total concentration samples are shown in Table 2 together with the results of Sadoc *et al.* [1, 2] obtained by using the curve fitting technique of EXAFS spectra. The structure factors of the 26.3 wt % Mn sample are in good agreement with those of the 30.0 wt % Mn sample, as a result of their similar EXAFS spectra and RDFs in Figs 9 and 10. The obtained neighbours were 9.3 aluminium atoms at the distance of 0.253 to 0.254 nm and 0.6 to 0.7 manganese atoms at the distance of 0.268 nm. Further, the structure factors of the amorphous phase prepared by the electrodeposition technique also correspond to the amorphous phase produced by the melt quenching method by Sadoc *et al.*

## 4. Discussion

### 4.1. *Distribution of f.c.c. and amorphous phases*

Generally, the integrated intensities of GIXD peaks increase nonlinearly for a mirror-surface sample with increasing X-ray glancing angle, because the X-ray refraction and reflection effects should be considered [15]. However, in uneven samples such as Al–Mn electrodeposits, both the refraction and reflection can be ignored and the integrated intensities increase almost linearly in the region of small glancing angles, if the linear absorption coefficient is constant, in other words, if the film is homogeneous in the through-thickness direction. The integrated intensities of the f.c.c. (1 1 1)-peak and amorphous halo increase nearly in proportion to glancing angle (0.2 to 2.0°) in the GIXD measurement as shown in Fig. 3. Therefore the f.c.c. crystalline and amorphous phases are distributed homogeneously in the through-thickness direction of Al–Mn electrodeposition films.

### 4.2. *Mn local concentration*

An f.c.c. crystalline lattice constant of aluminium solid solution with manganese has been shown to decrease with increasing Mn-amount [19]. The lattice constant of the f.c.c. crystalline phase in 11.2 wt % Mn is 0.4021 nm, as shown in Table 1, and is relatively small in comparison with that of the metastable f.c.c. containing 0.04 wt % Mn (0.40313 nm) [19]. This suggests that the f.c.c. crystalline phase contains a larger amount of manganese than the metastable phase. Therefore, it is thought that the f.c.c. phase in the 11.2 wt % Mn electrodeposit is supersaturated with manganese. On the other hand, the lattice constant of the f.c.c. phase in the 16.4 or 26.3 wt % Mn electrodeposit is smaller than that of pure aluminium (0.40494 nm) and larger than that of Al–0.004 wt % Mn (0.40399 nm) [19]. Therefore it is thought that the f.c.c. crystalline phases in 16.4 and 26.3 wt % Mn electrodeposits contain smaller amounts of manganese than 0.004 wt %.

*Table 2. Local structure of Al–Mn alloys (N, the number of neighbouring atoms, R, a distance to neighbouring atoms)*

| *Central atom* | *Sadoc et al.* [1, 2] | | | | | | *This work* | | | |
|---|---|---|---|---|---|---|---|---|---|---|
| | *Icosahedral* $Al_{86}Mn_{14}$ (24.9 *wt % Mn*) | | *Amorphous* $Al_{85}Mn_{15}$ (26.4 *wt % Mn*) | | *Decagonal* $Al_{80}Mn_{20}$ (33.7 *wt % Mn*) | | *Al–26.3 wt % Mn* | | *Al–30.0 wt % Mn* | |
| | *N* | *R*/nm | *N* | *R*/nm | *N* | *R*/nm | *N* | *R*/nm | *N* | *R*/nm |
| Mn | 1 Al | 0.2425 | | | | | | | | |
| | 5 Al | 0.255 | 9.5 Al | 0.2515 | 6.2 Al | 0.254 | 9.3 Al | 0.253 | 9.3 Al | 0.254 |
| | 2–3 Al | 0.272 | | | 2.5 Al | 0.271 | | | | |
| | 0.5–1 Mn | 0.262 | 0.5 Mn | 0.262 | 0.5 Mn | 0.258 | 0.7 Mn | 0.268 | 0.6 Mn | 0.268 |
| Al | – | – | 2 Mn | 0.254 | 2 Mn | 0.277 | – | – | – | – |
| | – | – | 9 Al | 0.280 | 10 Al | 0.280 | – | – | – | – |

The result from MEA in Fig. 7 also shows the decrease of manganese local concentration in f.c.c. crystalline phases with increasing manganese total concentration, although the analytical values are larger than the expected values from the lattice constant. The reasons for the larger values obtained by MEA are not well understood; one reason is the secondary excitation of manganese in the amorphous phase by X-rays from the f.c.c. crystalline phases, due to the small take-off angle (17.5°) in the MEA system.

As a result of partition between the f.c.c. and amorphous phases during the electrodeposition, the manganese local concentration in the f.c.c. phase decreases with increasing manganese total concentration. With increasing manganese total concentration, the decrease of manganese local concentration in the f.c.c. crystalline phases implies that a larger amount of manganese atoms tends to be partitioned into the amorphous phases.

### 4.3. *Local structure in the amorphous phase*

In the melt quenched Al–Mn alloy films the amorphous phase appears around 26.4 wt % Mn, and decagonal or icosahedral quasicrystalline phases form in greater or less manganese concentration. On the other hand, in the electrodeposits of Al–Mn alloys, amorphous and f.c.c. crystalline phases have been observed in the manganese concentration range between 11.2 and 30.0 wt %. The increase in manganese total concentration induces a decrease of the f.c.c. crystalline phase and an increase in the amorphous phase, resulting in the formation of a fully amorphous phase at 30 wt % Mn.

The manganese atom possesses ten first-neighbouring atoms in the icosahedron, amorphous phase, or decagon, ignoring their exact local structure. However, the local structure of the melt quenched amorphous phase is considered to resemble the icosahedral quasicrystalline phase $Al_{86}Mn_{14}$ better than the decagonal quasicrystalline phase $Al_{80}Mn_{20}$ in first-neighbouring atom distribution and distance, as reported by Sadoc *et al.* [1, 2]. In the amorphous phase of the electrodeposits the local structure obtained by our EXAFS analysis is in good agreement with that of the melt quenched amorphous phase by Sadoc *et al.* even in the wide range of manganese total concentration, i.e. between 16.4 and 30.0 wt % Mn. The result suggests that the manganese local concentration in the amorphous phase hardly changes with manganese total concentration. Therefore it is thought that the increase in manganese total concentration induces partition of manganese atoms more into the amorphous phase than into the f.c.c. crystalline phase during the electrodeposition.

## 5. Conclusions

Al–Mn alloy films containing 11–30 wt % Mn electrodeposited from eutectic molten chloride at a salt temperature of 473 K, were examined by using the GIXD method, HRTEM/EDS, and manganese *K*-edge EXAFS techniques, and the following results were obtained:

(i) The approximately linear relationships between the integrated intensities and the glancing angles in GIXD measurements have suggested homogeneous distributions of the f.c.c. and amorphous phases in the through-thickness direction.

(ii) The change of lattice constants of the f.c.c. crystalline phases has shown that the Mn-amount in the f.c.c. phase decreases with increasing manganese total concentration. This result was supported by the microarea elemental analysis.

(iii) The manganese local structures obtained by the EXAFS have indicated that the amorphous phase structure is almost the same among different manganese total concentration samples, and that the local structure is in good agreement with that of the melt quenched amorphous phase.

(iv) These results suggest that the increase in manganese total concentration may induce the partition of manganese atoms more into the amorphous phase than into the f.c.c. crystalline phase during electrodeposition.

## Acknowledgements

The authors wish to express their gratitude to Professor S. Yoshida, Drs T. Funabiki, H. Kanai and T. Tanaka for their comments upon EXAFS analysis, and Messrs K. Hanahusa and T. Tajima for assistance in part of the experiment.

## References

[1] A. Sadoc, A. M. Flank and P. Lagarde, *Physica B* **158** (1989) 60.
[2] A. Sadoc and J. M. Dubois, *J. Phys., Condens. Matter* **1** (1989) 4283.
[3] K. Masui, H. Nakamoto, S. Maruno, T. Kawaguchi and S. Sakakibara, *J. Non-Cryst. Solids* **124** (1990) 121.
[4] G. R. Stafford and B. Grushko, 176th Electrochem. Soc. Meeting (1989) 363.
[5] B. Grushko and G. R. Stafford, *Scripta Metall.* **23** (1989) 557.
[6] B. Grushko and G. R. Stafford, *Metall. Trans. A* **21** (1990) 2869.
[7] B. Grushko and G. R. Stafford, *Scripta Metall.* **23** (1989) 1043.
[8] M. Hansen, 'Constitution of Binary Alloys', McGraw-Hill, New York (1958) 111.
[9] T. Tsuda, H. Seto, J. Uchida, Y. Yamamoto, N. Usuki, T. Shiota, A. Shibuya and R. Noumi, SAE '90 Congress (1990) 900719.
[10] Y. Yamamoto, H. Seto, J. Uchida, T. Tsuda, A. Shibuya, R. Noumi, S. Fujita, T. Taguchi, J. Yoneda and K. Yanagi, AESF 6th Continuous Strip Plating Symposium (1990).
[11] T. Takayama and Y. Matsumoto, *Adv. X-ray Anal.* **33** (1990) 109.
[12] B. K. Teo, 'EXAFS: Basic Principle and Data Analysis', Springer-Verlag, New York (1986) 114.
[13] T. Tanaka, Y. Nishimura, S. Kawasaki, T. Funabiki and S. Yoshida, *J. Chem. Soc., Chem. Comm.* (1987) 506.
[14] S. Yoshida and T. Tanaka, *Adv. X-ray Chem. Anal. Japan* **19** (1988) 97.
[15] T. Takayama and Y. Matsumoto, *Bunseki Kagaku, Japan* **38** (1989) 500.

[16] M. Benfatto, C. R. Natoli, A. Bianconi, J. Garcia, A. Marcelli, M. Fanfoni and I. Davoli, *Phys. Rev. B* **34** (1986) 5774.
[17] T. Miyanaga, N. Matsubayashi, I. Watanabe and S. Ikeda, *Adv. X-ray Chem. Anal. Japan* **19** (1988) 119.
[18] A. D. I. Nicol, *Acta Crystallogr.* **6** (1953) 285.
[19] W. B. Pearson, 'A Handbook of Lattice Spacings and Structures of Metals and Alloys', Pergamon Press, Oxford (1967) 574.